Investigation of a $Cr_{42.2}Fe_{57.8}$ alloy prepared by mechanical alloying

2006 J. Phys.: Condens. Matter 18 3263

(http://iopscience.iop.org/0953-8984/18/12/008)

INSTITUTE OF PHYSICS PUBLISHING JOURNAL OF PHYSICS: CONDENSED MATTER

J. Phys.: Condens. Matter **18** (2006) 3263–3276 doi:10.1088/0953-8984/18/12/008

Investigation of a $Cr_{42.2}Fe_{57.8}$ alloy prepared by mechanical alloying

B F O Costa[1], S M Dubiel[2,3] and J Cieślak[2]

[1] Physics Department, University of Coimbra, 3004-516 Coimbra, Portugal
[2] Faculty of Physics and Computer Science, AGH University of Science and Technology, 30-059 Krakow, Poland

E-mail: dubiel@novell.ftj.agh.edu.pl

Received 12 December 2005, in final form 19 February 2006
Published 7 March 2006
Online at stacks.iop.org/JPhysCM/18/3263

Abstract

A $Cr_{42.2}Fe_{57.8}$ nano-crystalline alloy prepared by mechanical alloying for 100 h in argon atmosphere was investigated with Mössbauer spectroscopy (MS), differential scanning calorimetry (DSC), SQUID magnetometry and x-ray diffraction (XRD) techniques. Evidence was found that the final product was composed of two crystalline phases, namely (a) $Cr_{45}Fe_{55}$ with an abundance of ∼50% and (b) $Cr_{86.5}Fe_{13.5}$ with an abundance of ∼15%, and an amorphous phase having two crystallization temperatures: one at $T_{C1} \approx 870$ K and another one at $T_{C2} \approx 920$ K. The results prove that the milling process has led both to a partial amorphization and to phase decomposition into Fe-rich and Cr-rich phases.

1. Introduction

There are many good reasons that mechanical alloying (MA), also known as mechanical milling, has attracted much interest in recent years. One of them is the fact that it is an easy way to form materials in the nano-scale range. Such materials are of a great technological and scientific interest due to their physical properties, often very different from those of their conventional polycrystalline counterparts, as well as due to their actual and potential applications.

Other good reasons for the use of MA comprise synthesis of alloys of otherwise immiscible elements, extended solid solutions or amorphous materials to name just a few most significant.

The Fe–Cr system, the subject of the present study, is perhaps the best example of the use of MA in fabrication of amorphous state, as it seems to be one of the three known ways—the other two being thermal evaporation with a very low deposition rate followed by long-term annealing of co-deposited alloys, and the layer-by-layer procedure to prepare films—of achieving such a

[3] Author to whom any correspondence should be addressed.

state in the Fe–Cr system [1, 2]. Formation of amorphous Fe–Cr alloy directly from the melt has not been observed due most likely to the small difference in the atomic radii of Fe and Cr atoms.

One of the experimental methods that have proved to be useful in the study of MA in the Fe–Cr system and its products is Mössbauer spectroscopy (MS). Thanks to the high sensitivity of hyperfine parameters to coordination number and crystal field, the disordered (amorphous) state can be distinguished from the ordered one (crystalline), which is especially important in the case of the nano-crystalline Fe–Cr system, where the x-ray diffraction (XRD) method fails to distinguish unambiguously between amorphous, nano-crystalline and phase-separated Fe-rich and Cr-rich phases. However, despite this ability of MS and numerous studies carried out on Fe–Cr samples prepared by MA [1, 3–8, 10], there are still open questions to be answered. Such an unclear situation follows in our opinion from the fact that the milling process was carried out in various laboratories in different milling conditions in terms of number of balls, powder to ball ratio and speed of rotation. As is known, all these factors can influence the rate of mixing, size of grains and final phases. Although in most experiments the milling process started from elemental powders, there are also examples where a polycrystalline alloy was used as the starting material [1]. Based on the available results it seems to be certain that there is a basic difference in the final product obtained by MA in a vacuum and that synthesized in a different atmosphere (mostly argon). While the latter always results in a paramagnetic component at room temperature (RT), the former product is free of it [10]. This is an important difference, as the paramagnetic component and its origin have been the most debated issue. The component has been frequently regarded as the proof for the existence of the amorphous state in the Fe–Cr alloy produced by MA, although its interpretation given by various authors sometimes varies significantly. For example, Xia *et al* by recording Mössbauer spectra both at RT and at liquid helium temperature (LHT) on the samples milled for long enough time have shown that the paramagnetic line is in fact a doublet, which is a feature characteristic of the amorphous state [1, 5]. On the other hand, Fnidiki *et al* analysed their spectra only in terms of the hyperfine field distribution, i.e. they treated an entire spectrum as magnetic with two components: a magnetic one due to a crystalline core of grains and a paramagnetic one related to a non-magnetic inter-granular zone [6, 7]. Yet another approach and interpretation can be found in the paper by Bentayeb *et al* [8]. These authors treated the paramagnetic sub-spectrum as a single line and associated it with two paramagnetic phases: α' and γ.

In these circumstances, more experimental results are necessary and justified to gain more insight into the problem. In this paper we present and describe our results obtained with various techniques, namely MS, XRD, differential scanning calorimetry (DSC) and magnetic SQUID magnetometry on a $Cr_{42.2}Fe_{57.8}$ sample prepared by MA of elemental powders for 100 h.

2. Experimental details

The nano-crystalline sample was prepared by mechanical alloying using a planetary mill (Fritsch P-6) at a rotating speed of 500 rpm, equipped with a hardened steel vial (80 ml) and balls (five balls with 20 mm diameter each) with mixtures of powders of Fe (99.0+%, grain size 60 μm) and Cr (99.0+%, grain size 45 μm) in argon atmosphere. The weight of the powder was 7.35 g and the powder-to-ball weight ratio was 1:20. The total milling time was 100 h, interrupted for 15 min every hour.

The composition of the sample was determined by microprobe analysis and the result gave $Cr_{42.2}Fe_{57.8}$. Oxygen and nitrogen were determined by combustion of the sample in a LECO machine. There was no trace of O_2 or N_2 in the starting powders. The sample after milling showed contents of N_2 of 3.5 at.% and of O_2 of 3.2 at.%.

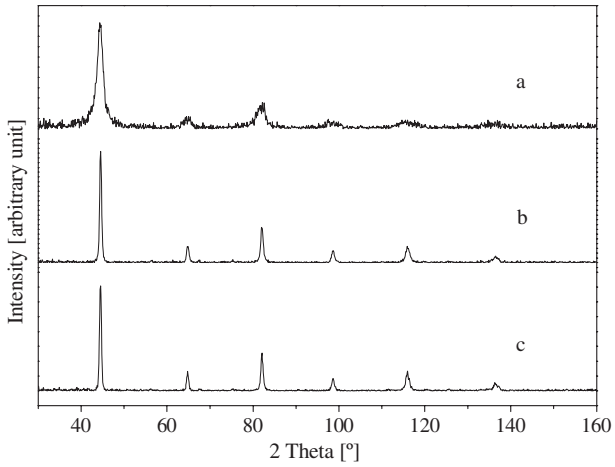

Figure 1. X-ray diffractograms (Cu Kα radiation, $\lambda = 0.158\,184$ nm) recorded at RT on samples (a) milled for 100 h and (b) then annealed at 873 K for 6 min, (c) annealed at 873 K for 6 min and afterwards annealed at 923 K for 6 min.

For the reasons explained later in the paper, the sample was annealed at 873 K for 6 min and after that it showed 2.0 and 1.0 at.% of N_2 and O_2, respectively.

The sample was studied by MS, XRD, DSC and SQUID techniques. Mössbauer spectra were recorded at room temperature, 83 K and 4.2 K in transmission geometry with the spectrometer operating in conventional constant acceleration mode. A ^{57}Co source in Rh matrix was used as the source of 14.4 keV gamma rays. Spectra were analysed by various approaches yielding a hyperfine magnetic field distribution (HFD), quadrupole splitting distributions (QSD) and single lines. Lorentzian line-shapes were assumed in this procedure. The XRD patterns were obtained using Cu Kα radiation ($\lambda = 0.154\,184$ nm) at room temperature. The mean crystallite sizes and micro-strains were obtained from the widths of x-ray diffraction peaks using the Williamson–Hall method [9]. DSC was used to characterize the sample, from room temperature to 1070 K, at the heating rate of 40 K min^{-1} in argon atmosphere. Saturation magnetization was determined with a SQUID magnetometer at a temperature of 4.2 K.

3. Results and discussion

3.1. XRD

The XRD pattern of the as-milled sample recorded at RT is shown in figure 1(a), while that of the sample annealed at 873 K for 6 min is shown in figure 1(b). In figure 1(c) the pattern of the sample annealed at 873 K and again at 923 K for 6 min is shown. The positions of the peaks are in all cases characteristic of a bcc phase, but the peaks from the as-milled sample (figure 1(a)) are broadened relative to those characteristic of a micro-crystalline sample. The broadening was accounted for by the size of grains and micro-strain following [10], and analysis resulted in 5.4 nm for the mean crystalline size, $\langle d \rangle$, and 1.8% for the micro-strain. However, as can be seen in figure 2, showing the strongest peak in figure 1(a) in an enlarged scale, the peak is not symmetric and can be fitted with two Lorentzian-shaped lines; one very broad, which constitutes ∼40% of the peak area, and which can be associated with an amorphous phase, and the other narrower, which can be assigned to a crystalline phase. If we take into account only the narrower peak, then the average size of grains is 7.3 nm and the micro-strain is 0.5%.

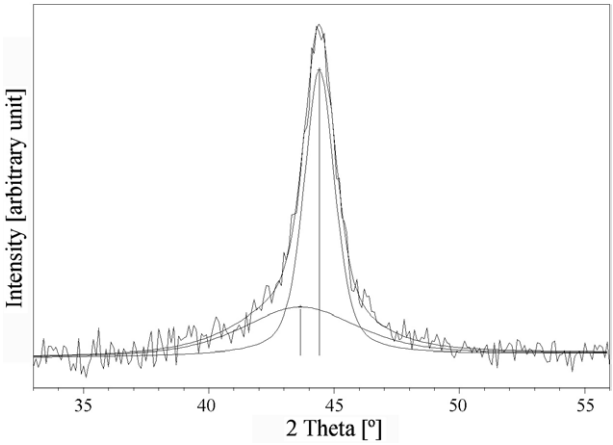

Figure 2. First peak of the x-ray diffractogram shown in figure 1(a) as analysed with two Lorentzians. The broader one is ascribed to an amorphous phase.

Taking into account these grain size values, one can estimate the volume fraction, V_g, of the amorphous phase or the phase related to the grain surface and/or grain boundary (GB) zone. For this purpose, the following formula can be used:

$$V_g = \frac{3e}{\langle d \rangle} \tag{1}$$

where e is the effective thickness of the GB zone. Making a customary assumption $e = 1$ nm, one arrives at $V_g = 56\%$ for $\langle d \rangle = 5.4$ nm or at 41% for $\langle d \rangle = 7.3$ nm. The latter figure agrees very well with the corresponding figure obtained from the diffraction peak.

3.2. Mössbauer

3.2.1. Spectrum analysis. The Mössbauer spectra recorded at three different temperatures, namely 300, 83 and 4.2 K, are shown in figure 3. As can be seen, they are quite similar to each other and can be viewed as composed of two sub-spectra: (a) a pseudo-single-line sub-spectrum in the centre and (b) a broad magnetic sub-spectrum. Others have also observed such a kind of spectra for mechanically prepared Fe–Cr alloys in argon atmosphere [1, 3–8], but not in a vacuum [9]. The basic question that arises is the interpretation of the two component sub-spectra. Whilst the magnetic one has been uniquely associated with the crystalline core of nano-grains, there are various interpretations of the pseudo-single-line sub-spectrum as already mentioned in the introduction. It seems that such an unclear situation partly follows from the method of spectrum analysis used by different authors, and partly because some investigators measured their spectra only at RT [6–8], which, as will be shown below, leads to not quite the correct interpretation. Recording spectra at different temperatures, and in particular at liquid nitrogen temperature (LNT) and LHT, as is the case here, is crucial for the correct analysis and interpretation of the pseudo-single-line contribution.

In order to show how the method of spectrum analysis influences the spectral parameters, and consequently the interpretation of the results, several possible approaches were used in the present analysis of the spectra. Before they are presented, let us notice that *a priori* the pseudo-single-line sub-spectrum can have the following origins: (i) superparamagnetism, (ii) grain boundaries and/or grain interfaces, (iii) Cr-rich α' phase and (iv) σ-Fe–Cr phase. All these

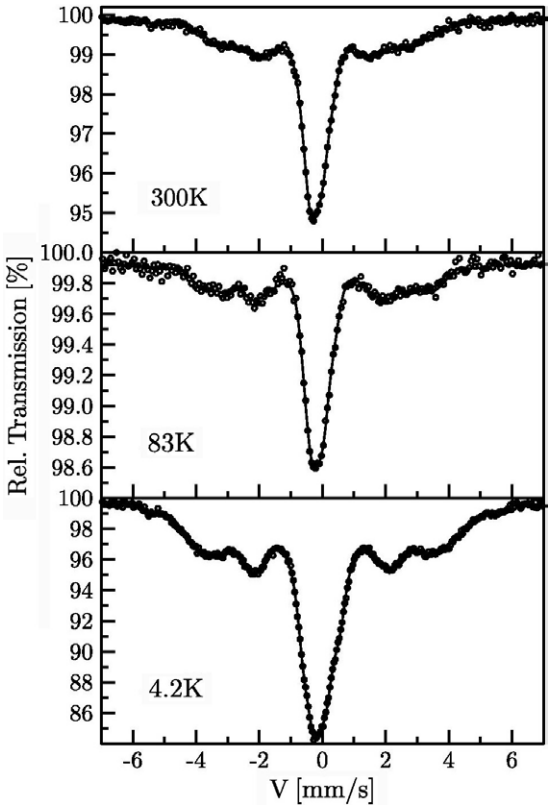

Figure 3. ^{57}Fe Mössbauer spectra recorded on the as-milled sample at the temperatures shown. The solid lines are the best-fit spectra.

Table 1. The best-fit spectra parameters obtained with procedure I. A is the spectral area, IS is the isomer shift, G is the line-width of the single line, and $\langle B \rangle$ is the average hyperfine field of the magnetic sub-spectrum.

	Single line			HFD		
T (K)	A (%)	IS (mm s^{-1})	G (mm s^{-1})	A (%)	IS (mm s^{-1})	$\langle B \rangle$ (T)
300	62	−0.085	0.80	38	−0.055	18.7
83	60	−0.045	0.76	40	−0.02	20.1
4.2	51	0.015	1.00	49	0.02	22.8

possibilities are feasible in the light of the Fe–Cr system phase diagram and our knowledge of nano-crystalline Fe–Cr alloys prepared by MA.

In the first approach (procedure I) the spectra were analysed assuming they are composed of a single line superimposed on a broad sextet with a distribution of the hyperfine field (HFD). The spectra could have been successfully fitted in this way and the best-fit spectral parameters derived from this procedure are displayed in table 1. The HFD histograms are shown in the top row in figure 4.

As can be seen, the isomer shifts of the two sub-spectra, IS, differ meaningfully from each other, which permits us, already at this stage, to eliminate superparamagnetism as a possible

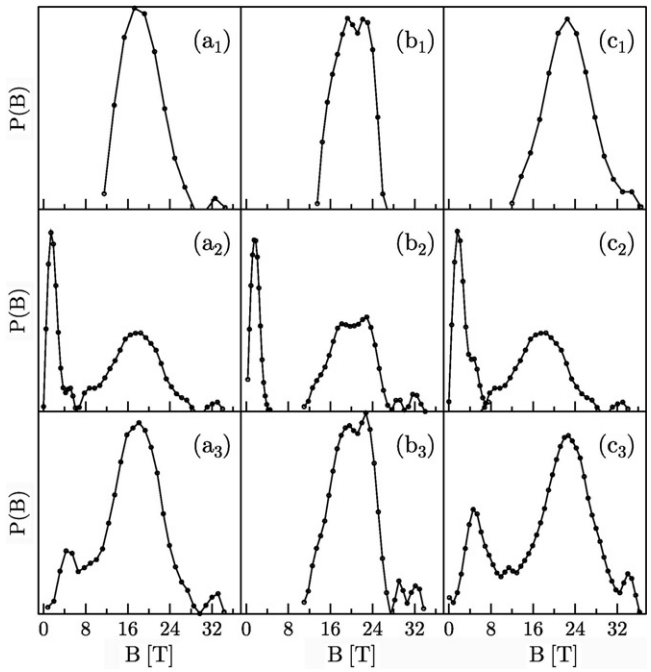

Figure 4. HFD histograms as obtained from the spectra shown in figure 3 with different fitting procedures: procedure I (subscript 1), procedure II (subscript 2) and procedure III (subscript 3). The labels *a*, *b* and *c* stand for the temperatures 300, 83 and 4.2 K, respectively.

origin of the single-line sub-spectrum. Furthermore, its full line width at half maximum, G, is larger by a factor ∼3 than the typical line width of crystalline materials in a paramagnetic state, hence this line here cannot be due to any paramagnetic crystalline bcc phase. It could eventually be due to the σ-FeCr phase, but the value of IS $= -0.085$ mm s^{-1} excludes this possibility [11]. Hence, this phase cannot be present here, but its formation is quite unlikely anyway because of the low temperature during MA. For polycrystalline Fe–Cr alloys, the σ phase can precipitate between 800 and 1100 K. The increase of temperature of powders during MA is believed to be less than 300 K [12], and in MA of extended Cr–Sn solid solutions it was estimated as ∼230 K [13]. This makes the temperature of powders during MA some 200 K too low for the σ-FeCr phase to form. In summary, the first approach of our spectrum analysis has excluded superparamagnetism as a possible reason for the pseudo-single-line sub-spectrum. Also α' and σ phases cannot be solely responsible for this sub-spectrum. From the temperature behaviour of the line width, it can be further concluded that, at least down to 83 K, the phase related to this sub-spectrum cannot be magnetic. It should be noticed that ∼2% magnetic contribution with $\langle B \rangle \approx$ 33–34 T was revealed. It can be identified as due to α-Fe. However, lowering T down to 4.2 K has resulted in a decrease of the intensity of the sub-spectrum by ∼10%. Nevertheless, ∼50% has survived as non-magnetic even at 4.2 K with almost unchanged value of G. It may be either crystalline with a lower-than-cubic symmetry (σ phase) or non-crystalline, i.e. amorphous. To shed some additional light on this question, the spectra were fitted with other approaches. Firstly, in procedure II, the spectra were analysed in terms of the HFD histograms, namely it was assumed that each spectrum is composed of two distributions: low field responsible for the central part of the sub-spectrum and high field responsible for the well split sub-spectrum. The HFD histograms resulting from this procedure

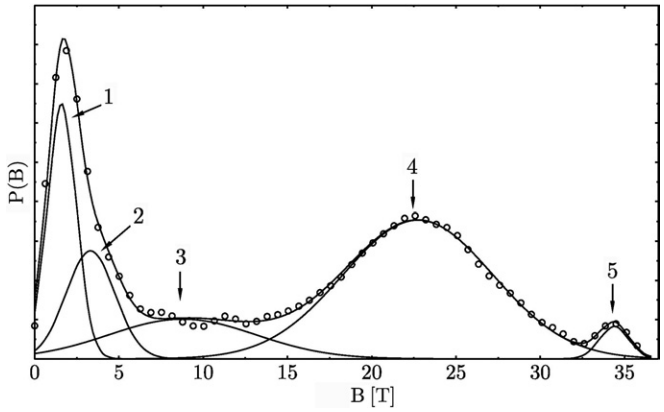

Figure 5. HFD histogram obtained from the spectrum recorded at 4.2 K with procedure IIA. The arrows indicate five peaks into which the histogram can be separated.

Table 2. Spectral parameters derived from procedure II (two HFDs). The meanings of the symbols used are the same as those in the caption of table 1.

	Low field			High field		
T (K)	A_1 (%)	IS_1 (mm s^{-1})	$\langle B_1 \rangle$ (T)	A_2 (%)	IS_2 (mm s^{-1})	$\langle B_2 \rangle$ (T)
300	49	−0.07	2.0	51	−0.03	17.6
83	49	−0.04	1.8	51	0.02	20.4
4.2	48	0.02	4.3	52	0.06	22.7

indicated with subscript 2 are shown in figure 4, while the spectral parameters are displayed in table 2.

It should be mentioned that for $T = 300$ and 83 K the spectra could have been well fitted with two HFDs whose field ranges were separated from each other. However, in order to get a good fit for the spectrum measured at 4.2 K one has to allow overlapping of the two field ranges. In other words, at 4.2 K a new field component has appeared between the two HFDs. In order to better account for this effect, the 4.2 K spectrum was fitted with procedure IIA, assuming a continuous HFD in the whole field range and a linear correlation between B and IS. This procedure has resulted in a very good fit and the HDF obtained is presented in figure 5. It is clear from this that in the gap between the low-field and the high-field peaks seen in the HFD derived from the spectrum recorded at 83 K a new component has appeared. As can be seen, the whole HFD histogram can be separated into five peaks whose spectral parameters are displayed in table 3. The main difference between the two-HFD procedure and the continuous HFD procedure is a decrease of the low-field component whose contribution according to procedures I and II was equal to ∼50%. As follows from table 3, it decreased to ∼30% and a new ∼15% component with $\langle B \rangle \approx 9$ T has appeared. The values of $\langle B \rangle$ for peaks 1 and 2 may indicate that the underlying phases are not magnetic. Low values of $\langle B \rangle$ can be alternatively accounted for by the quadrupole splitting. For this purpose, the spectra were fitted with procedure III, i.e. assuming a superposition of two distributions: HFD and QSD (distribution of quadrupole splitting), the latter responsible for the non-magnetic component. The spectral parameters derived from procedure III are displayed in table 4, the HDF histograms obtained presented in figure 4 as the bottom row and the QSD histograms in figure 6.

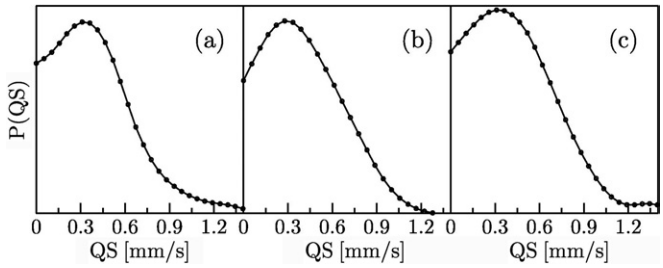

Figure 6. QSD histograms as obtained from the spectra shown in figure 3 with procedure III for (a) $T = 300$ K, (b) $T = 83$ K and (c) $T = 4.2$ K.

Table 3. Spectral parameters of five peaks in the HFD histogram shown in figure 5. The meanings of the symbols are the same as in table 1.

Peak no	A (%)	IS (mm s^{-1})	$\langle B \rangle$ (T)
1	18.5	−0.10	1.6
2	13	−0.095	3.3
3	14.5	−0.07	8.8
4	51.5	−0.015	22.7
5	2.5	0.005	34.4

Table 4. Spectral parameters derived from procedure III (HFD + QSD). ⟨QS⟩ refers to the average quadrupole splitting. The meanings of other symbols are the same as in table 1.

	QSD			HFD		
T (K)	A (%)	IS (mm s^{-1})	⟨QS⟩ (mm s^{-1})	A (%)	IS (mm s^{-1})	$\langle B_1 \rangle$ (T)
300	44	−0.08	0.40	56	−0.03	16.4
83	49	−0.04	0.40	51	0.03	20.4
4.2	26	0.02	0.42	51	0.07	22.4
				23		5.1

In all procedures a residual contribution (∼2%) identified as α-Fe was found.

3.2.2. Spectral parameters. Let us first discuss the results concerning the central subspectrum. All three methods of spectrum analysis gave a similar amount, A, of this contribution at 300 and 83 K. However, the A-value yielded by the first method—60%—is larger by ∼10% than those evaluated from the other two procedures. This means that applying the former probably results in an overestimation of the 'paramagnetic' fraction. Lowering T to 4.2 K has resulted in a decrease of the 'paramagnetic fraction' by ∼10% according to the data in table 1, by ∼15% according to the data in table 3 and by ∼25% according to the data in table 4. In other words, it follows that at 4.2 K ∼ 25% to ∼50% of the sample remains in a non-magnetic phase. A better agreement between all three methods exists as far as the isomer shift, IS, of the 'paramagnetic' and magnetic phases is concerned. As follows from tables 1, 2 and 4, at RT IS ranges between −0.085 and −0.07 mm s^{-1} for the 'paramagnetic' component and between −0.05 and −0.03 mm s^{-1} for the magnetic one. Good agreement also holds for the values of the average hyperfine field, $\langle B \rangle$.

The difference by a factor of ∼2 in A-values clearly shows that some results of spectral analysis of the nano-crystalline Fe–Cr alloys significantly depend on the method used in the

analysis of the spectra. As the results obtained with the last two procedures (II and III) are in good agreement, we will neglect procedure I results in the following discussion, and assume that at 4.2 K 25–35% of the sample is nonmagnetic or weakly magnetic ($\langle B \rangle \approx 2$ T), i.e. 15–25% has become magnetic below 83 K.

Let us first discuss the results obtained for the magnetic sub-spectrum, which seem to be clearer. Their spectral parameters, i.e. IS and $\langle B \rangle$ values, are characteristic of the crystalline Fe–Cr alloys obtained in a conventional way, i.e. by arc melting [14]. For such alloys monotonic relationships between $\langle B \rangle$ and the alloy composition was found [15–17], so they can be used here for the evaluation of the composition of this magnetic phase, usually associated with the core of the nano-crystals. It should be added that according to [15] one uses 4.2 K $\langle B \rangle$-values, while those recorded at RT are needed when using formulae from [16, 17]. So taking into account the data from table 2 we arrive at $x_{Fe} = 54$, 43 and 55 using [15–17], respectively, while using the data from table 4 yields correspondingly $x_{Fe} = 44$, 38 and 54. It should be recalled here that $x_{Fe} = 58$ was found from the microprobe analysis as the Fe content of the alloy. So the question of the magnetic sub-spectrum seems to be rather clear, although its exact composition varies depending on the method used to its determination. What remains to be solved is the nature of the non-magnetic or very weakly magnetic component ($A \approx 25$–35%) as well as that which became weakly magnetic on lowering T down to 4.2 K ($A \approx 15\%$). Some insight into the issue can already be gained from the HFD histogram derived from the 4.2 K spectrum, which is shown in figure 5. Its structure is more complex than that found at 83 K. Namely, five peaks can be distinguished: number 5 at 34 T due to α-Fe (2%), number 4 at 22.7 T due to α-Fe–Cr (52%), number 3 at 8.8 T (15%), number 2 at 3.3 T (13%) and number 1 at 1.6 T (18%). In order to identify peak number 3 we notice its feature, i.e. a broad distribution ranging from 0 to 20 T with the average value of $\langle B \rangle = 8.8$ T and its abundance of 15%. The latter value together with the fact that the amount of the 'paramagnetic' phase has decreased just by ~15% while the magnetic phase remained constant allows the conclusion that this peak represents the phase that has become magnetic due to the decrease of T from 83 to 4.2 K. Its magnetic features, i.e. the broad distribution and the $\langle B \rangle$-value, allow us to associate it with crystalline Cr-rich Fe–Cr alloys [18, 19], and estimate the concentration of Fe, $x_{Fe} = 13$–14 at.% [17]. Consequently, we think that we have found for the first time experimental evidence for such a phase (Cr-rich α') in MA Fe–Cr alloys. Its existence is, in fact, a logical consequence of the phase-decomposition (de-mixing) process, which was sometimes suggested to take place during MA of these alloys. However, in the literature the only argument in favour of this phenomenon was an enhancement of $\langle B \rangle$ observed after crystallization [1, 7]. This effect was also observed in this study as described below.

The final unsolved question is related to peaks numbers 1 and 2 in figure 5. It seems unlikely that they are magnetic, because the values of $\langle B \rangle$ ascribed to them hardly depend on T between 300 and 4.2 K. Such a feature of a Mössbauer spectrum is rather characteristic of the quadrupole splitting, QS, which, in this case, could be due to amorphous state. The existence of such a state in MA Fe–Cr alloys, sometimes called disordered state, was already postulated in several papers, and was usually associated with grain boundaries. In available literature, there are some good arguments in favour of such an interpretation, like direct observation of a quadrupole doublet on samples milled for long periods [1], existence of exothermic peaks in DSC-curves [1, 7] and, partly, broadened XRD patterns. As will be demonstrated below, all these signatures have also been found in our sample. As already discussed above, the 'paramagnetic' sub-spectrum observed at all T in this study could have been well accounted for by the distribution of QS, which for the three spectra is shown in figure 6 as obtained with procedure III. QS-values range between 0 and 1.0 mm s^{-1}, which is typical of amorphous Fe-based alloys [3, 7]. The two low-field peaks in the 4.2 K HFD shown in figure 5, i.e. number 1

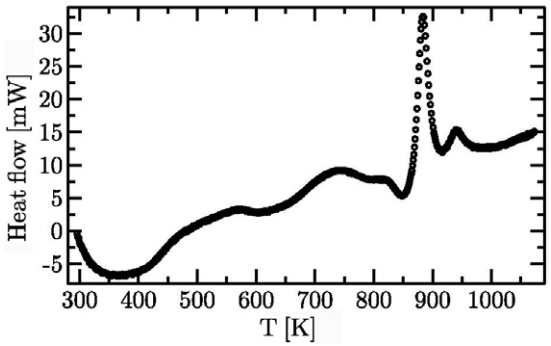

Figure 7. DSC trace of the studied sample milled for 100 h.

and number 2, may be well accounted for by two distributions of QS related to two amorphous phases: one rich in Fe, another rich in Cr. The low values of the isomer shift ascribed to these phases could also well fit to the fact that IS of the amorphous state is more negative than that for crystalline state of similar composition [1]. Taking further into account that for Fe–Cr alloys IS decreases with Cr content [11, 20], one can speculate that peak number 1 in figure 5 is due to the Cr-rich amorphous phase and number 2 to the Fe-rich one.

3.3. DSC and SQUID

Both calorimetric and magnetic studies can contribute to our understanding of amorphous phases as they have turned out to be useful tools in distinguishing between crystalline and amorphous states. Differential scanning calorimetry (DSC) was used in the past to investigate Fe–Cr alloys prepared by MA [3, 6]. In figure 7, a DSC curve recorded on our as-milled sample in the temperature interval of 295 to 1070 K is given. One can see two exothermic narrow peaks, one at $T_{C1} \approx 870$ K and another, smaller, at $T_{C2} \approx 920$ K, which can be associated with the crystallization processes. The reaction enthalpy, ΔH, was estimated at $-16\,577$ J kg^{-1} for the first process and -2721 J kg^{-1} for the second one. In the DSC analysis of amorphous solids, one amorphous phase can have more than one peak [21, 22]. Conversely, two amorphous phases could have one DSC peak, so this two-peak structure observed in the present study does not necessarily mean that we have two amorphous phases in our 100 h milled sample, one rich in Fe, another rich in Cr, although it does not exclude such a possibility. In our opinion it is quite likely that in the present case the amorphous phase consists of Fe-rich and Cr-rich regions. A similar two-peak feature in the DSC curve was observed by Xia *et al* [1], but not by Fnidiki *et al* [7], who recorded only one peak at about T_{C1}. They also revealed that ΔH was linearly correlated with the amount of paramagnetic phase. This behaviour, together with the fact that $T_C \approx T_{C1}$ and T_{C2}, can be used to estimate the fraction of the paramagnetic phase in our sample from our $\Delta H = -19\,298$ J kg^{-1}. Doing so we arrive at ∼35%, a figure that is within the 25%–35% range as estimated from our 4.2 K Mössbauer spectrum. A broad peak which can be recognized in the DSC curve at $T \approx 720$ K can be treated as a mixture of the heat effect of grain growth and recovery of atomic disorder [23].

To see the effect of the process that takes place at T_{C1}, a sample was annealed in vacuum at 873 K for 6 min. After such treatment, the sample was investigated with XRD, MS and SQUID techniques.

The XRD pattern obtained after the annealing is shown in figure 1(b). It is characteristic of the bcc structure. From the width of peaks, we have determined the mean crystalline size and

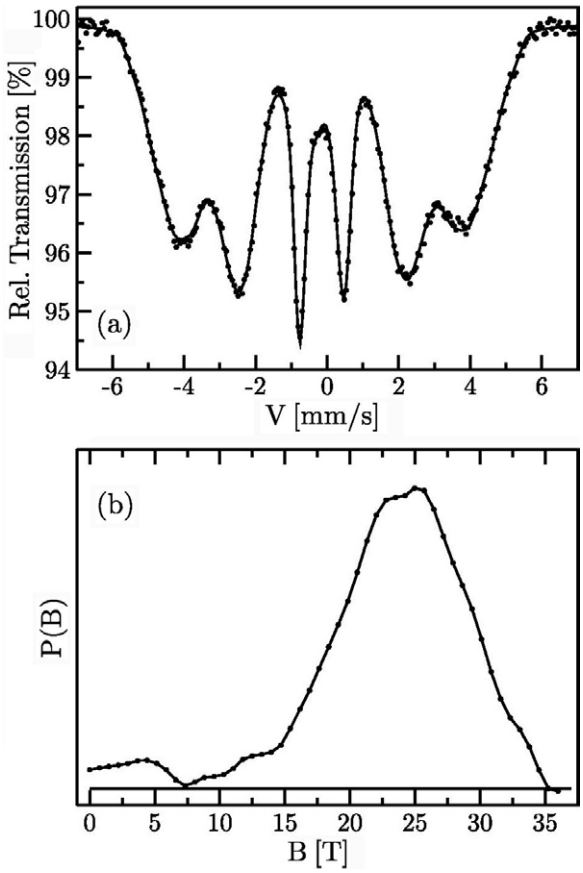

Figure 8. (a) Mössbauer spectrum recorded at RT on the sample annealed at 873 K for 6 min, and (b) the corresponding HFD histogram.

micro-strain to be 24.4 nm and 0.42%, respectively. Saturation magnetization as determined with the SQUID magnetometer at 4.2 K was equivalent to 2.02 μ_B/atom Fe which agrees well with the value of bulk alloys of corresponding composition [24]. This should be compared with 1.18 μ_B/atom obtained from the as-milled sample, a value characteristic of an amorphous state and/or micro-crystalline alloys [25]. Figure 1(c) shows the pattern for the sample annealed at 873 K and then again at 923 K for 6 min. From the peak widths, the mean crystalline size and strain are 23.5 nm and 0.30%, respectively.

Next, the Mössbauer spectrum was recorded on the annealed sample at RT. It can be seen in figure 8 together with the corresponding HFD histogram. Its spectral parameters obtained are $\langle B \rangle = 23.2$ T and $\langle \mathrm{IS} \rangle = -0.04$ mm s^{-1}. The increase of $\langle B \rangle$ by 5–6 T with respect to the as-milled sample, which corresponds to a 5–6% increase in Fe content, is another signature of the phase-decomposition process that has taken place during MA. A small fraction (∼4%) of a low-field component with $\langle B \rangle \approx 3$ T and $\langle \mathrm{IS} \rangle = -0.12$ mm s^{-1} can be seen. It may be related to the second Cr-rich amorphous phase (T_{C2} peak in the DSC curve in figure 7). This supposition seems to be correct in the light of the Mössbauer spectrum recorded at RT on a homogenized sample of crystalline $Cr_{40}Fe_{60}$ alloy—see figure 9(a)—and the related HFD histogram—see figure 9(b). The latter is free of the low-field component. Finally, the sample annealed at 873 K

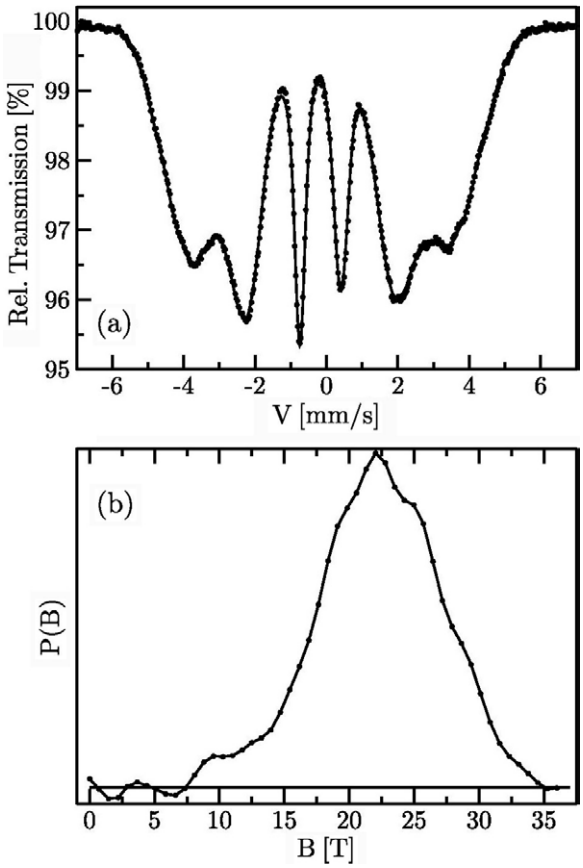

Figure 9. (a) Mössbauer spectrum recorded at RT on a crystalline homogeneous sample of $Cr_{40}Fe_{60}$ alloy, and (b) the corresponding HFD histogram.

was again annealed at $T_{C2} = 923$ K for 6 min, and an RT Mössbauer spectrum was recorded on it—see figure 10(a). The corresponding HFD histogram is presented in figure 10(b). Its spectral parameters remained unchanged in comparison with those presented in figure 8(b), except for the amount of the small-field component, whose contribution increased by ∼2%. Such an increase can be due either to uncertainty in the spectrum evaluation caused by a small change of the spectral parameters of the paramagnetic component due to crystallization of the amorphous Cr-rich phase or, which is also possible, to the precipitation of a small fraction of the σ phase. However, the XRD pattern recorded after the second annealing—see figure 1(c)—does not show any trace of this phase.

4. Conclusions

Investigation of a $Cr_{42.2}Fe_{57.8}$ alloy prepared by MA in argon atmosphere over 100 h with the use of MS, XRD, DSC and SQUID permits us to draw the following conclusions.

(1) The as-milled sample has a nano-crystalline structure.
(2) The as-milled sample is magnetically, structurally and chemically heterogeneous.
   (a) Between 83 K and RT, ∼50% is magnetic (α-Fe–Cr) and ∼50% non-magnetic.

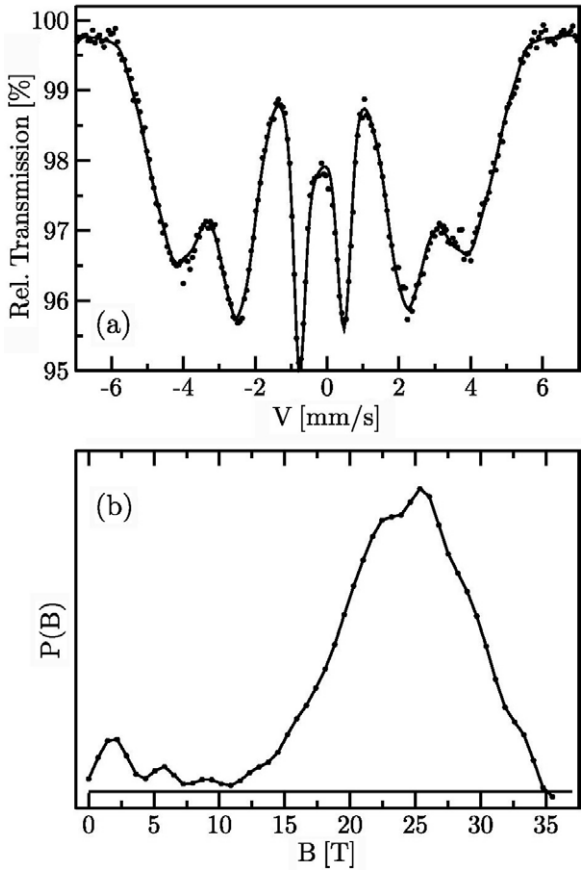

Figure 10. (a) Mössbauer spectrum recorded at RT on the sample annealed at 923 K for 6 min, and (b) the corresponding HFD histogram.

(b) At 4.2 K, ∼65% is magnetic—the ∼15% increase due to α' phase containing 13–14 at.% Fe, and ∼35% is non-magnetic.

(c) The non-magnetic phase (∼35%) is amorphous and probably consists of Fe-rich and Cr-rich components which crystallize at ∼870 K and ∼920 K, respectively.

(3) After annealing for 6 min at 873 K, the sample became crystalline with the average size of grains equal to 24.4 nm.

(4) After annealing at 873 K, the magnetic moment increased from 1.18 μ_B/Fe atom to 2.02 μ_B/Fe atom and the average hyperfine field from 17.6 to 23.2 T. The latter corresponds to Fe enrichment by 5–6%.

(5) Annealing at 923 K for 6 min did not practically affect the spectral parameters.

Acknowledgments

We wish to thank Dr Vitor Amaral from CICECO/Universidade de Aveiro for the magnetic measurements and Professor Walter Steiner from TU Wien for recording the 4.2 K Mössbauer spectrum. An anonymous referee is sincerely thanked for help in improving the language.

References

[1] Xia S K, Baggio-Saitovitch E, Rizzo Assuncao F C and Pena Rodrigues V A 1993 *J. Phys.: Condens. Matter* **5** 2729
[2] Levin A A, Meyer D C, Gorbunov A, Mensch A, Pompe W and Paufler P 2003 *J. Alloys Compounds* **360** 107
[3] Kuwano H, Ouyang H and Fultz B 1992 *Mater. Sci. Forum* **88–90** 537
[4] Ogino Y, Namba K and Yamasaki T 1993 *ISIJ Int.* **33** 420
[5] Xia S K, Baggio-Saitovitch E and Larica C 1994 *Phys. Rev.* B **49** 927
[6] Lemoine C, Fnidiki A, Lemarchand D and Teillet J 1999 *J. Phys.: Condens. Matter* **11** 8341
[7] Fnidiki A, Lemoine C and Teillet J 2002 *J. Phys.: Condens. Matter* **14** 7221
[8] Bentayeb F Z, Alleg S, Bonzabata B and Greneche J M 2005 *J. Magn. Magn. Mater.* **288** 282
[9] Shen G, Jiang D M, Lin F, Shi W Z and Ma X M 2005 *Physica* B **367** 137
[10] Williamson G and Hall W H 1952 *Acta Metall.* **1** 22
[11] Dubiel S M and Inden G 1987 *Z. Metallk.* **78** 544
[12] Davis R M, McDermott B and Koch C C 1988 *Metall. Trans.* A **19** 2867
[13] Le Caer G and Matteazzi P 1994 *Hyper. Interact.* **90** 229
[14] Dubiel S M and Zukrowski J 1981 *J. Magn. Magn. Mater.* **23** 214
[15] Kuwano H and Ono K 1977 *J. Phys. Soc. Japan* **42** 72
[16] Kuwano H 1985 *Trans. Japan Inst. Metall.* **26** 473
[17] Cieslak J, Dubiel S M and Sepiol B 2000 *J. Phys.: Condens. Matter* **12** 6709
[18] Dubiel S M, Sauer Ch and Zinn W 1985 *Phys. Rev.* B **32** 2745
[19] Herbert I R, Clark P E and Wilson G V H 1972 *J. Phys. Chem. Solids* **33** 979
[20] Kuwano H and Morooka Y 1980 *J. Japan Inst. Met.* **44** 1134
[21] Koeng K G, Sha W and Malinov S 2003 *Mater. Sci. Eng.* A **365** 212
[22] Guo Z, Koeng K G and Sha W 2003 *J. Alloys Compounds* **358** 112
[23] Yang H and Bakker H 1994 *Mater. Sci. Eng.* A **181/182** 1207
[24] Aldred A T 1976 *Phys. Rev.* B **14** 219
[25] Costa B F O, Le Caer G, Loureiro J M and Amaral V S 2006 *J. Alloys Compounds* at press